INSTITUTE OF PHYSICS PUBLISHING SUPERCONDUCTOR SCIENCE AND TECHNOLOGY

Supercond. Sci. Technol. **16** (2003) 484–491 PII: S0953-2048(03)55797-9

Effect of the precursor powders on the final properties of hot-forged Bi2223 textured discs

E Guilmeau, D Chateigner and J G Noudem

CRISMAT Laboratory, ISMRA, 6 Bd. Maréchal Juin, 14050 CAEN, France

E-mail: emmanuel.guilmeau@ismra.fr

Received 7 November 2002, in final form 15 January 2003
Published 24 February 2003
Online at stacks.iop.org/SUST/16/484

Abstract
The effect of precursor powder assemblage on the phase formation, crystallite orientation and transport critical current density of Bi2223 textured discs has been studied. We observe that starting powder composed of Bi2212 and secondary phases results in a stronger grain alignment than if composed of nearly pure Bi2223. SEM observations and XRD analyses show that the liquid phase produced during the sinter-forging step is essential to achieve sharp orientation distributions and high critical current densities.

1. Introduction

Sinter-forging methods are effective for obtaining bulk ceramics of $(Bi,Pb)_2Sr_2Ca_2Cu_3O_{10+x}$ (Bi2223) superconductor with a grain oriented texture. High texture strengths and critical current densities around 10 000 A cm^{-2} at 77 K in self-magnetic field have been obtained [1–3]. However, in various papers published on this subject, similar optimized transport properties for Bi2223 are reported. The composition of the starting powder is probably the main cause of such saturation, as sinter-forging techniques generally used starting pellets composed of highly pure Bi2223 powder. Thus, the typical sinter-forging process requires precise control of the experimental conditions to allow weak partial fusion of the Bi2223 phase, which produces enough liquid phase to allow sufficient grain rotation and sliding. This weak decomposition is difficult to control and generally leads to a decrease of the Bi2223 phase content [4].

An alternative route for the synthesis of highly textured Bi2223 discs was recently reported [5]. Here, instead of starting with a pure Bi2223 powder, we propose the use of calcined powders composed of Bi2212 and secondary phases such as Ca_2PbO_4, $CaCuO_3$ or CuO [6–10], in solid or liquid states, as starting components. As a result, at a high temperature, the plate-like grains of Bi2223 phase grow and reorient more easily because of the large amount of liquid in the powder [11, 12]. Preliminary results showed that critical current densities as high as 13 000 A cm^{-2} could be achieved using this alternative route. However, the characteristics of the best samples are still not optimized. The Bi2223 phase content is relatively low and must be increased in order to improve the critical current density, which may be accomplished by using different starting powder compositions and grain size distributions in order to increase powder reactivity, i.e. the Bi2223 phase formation kinetic.

The purpose of this study is to investigate the influence of starting precursor powders on the transport properties and texture quality of samples prepared by the sinter-forging method. A comparative analysis with previous studies will explain the role of the starting phase assemblage and grain size on the Bi2223 phase formation, grain alignment and superconducting properties.

2. Experimental details

All powders were prepared by the EDTA sol-gel method [13] using the nominal composition $Bi_{1.85}Pb_{0.35}Sr_2Ca_2Cu_{3.1}O_{10+\delta}$. However, the phase content in the powder and the grain size can be varied by using different heat treatments and intermediate grindings. Three types of powder, named powders A, B and C, have been produced by the following processes.

Process A. The raw powders were manually ground in an agate mortar, calcined under air at 820 °C for 24 h [14] and heat treated for several sintering steps. The sintering cycle, optimized in a previous work [15], was 845 °C/100 h, 845 °C/50 h and 838 °C/50 h with intermediate grindings between each sintering step. This heat treatment leads to a Bi2201-free Bi2223 powder with less than 6% of Bi2212, as determined by x-ray diffraction.

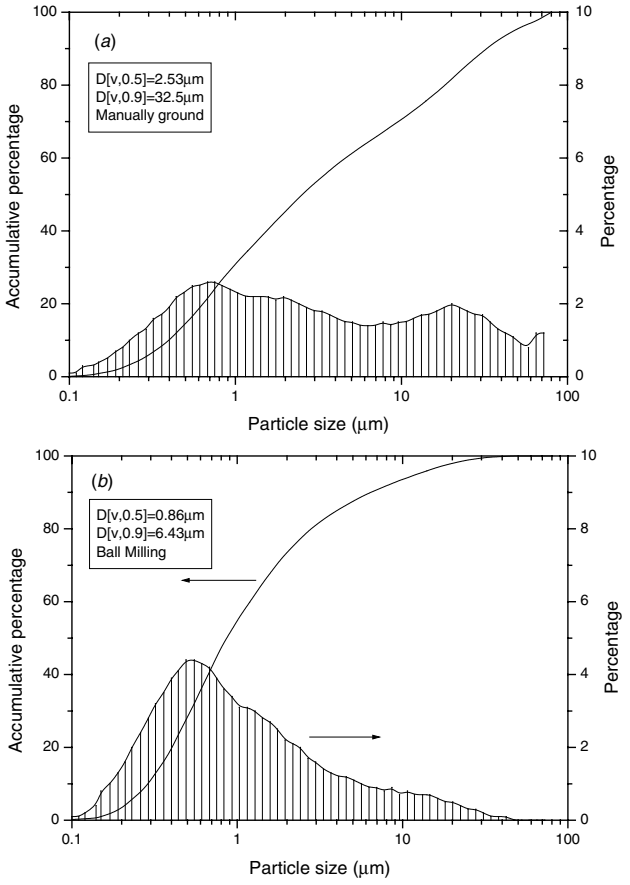

Figure 1. Particle size distributions of powders B (*a*) and C (*b*) before calcination.

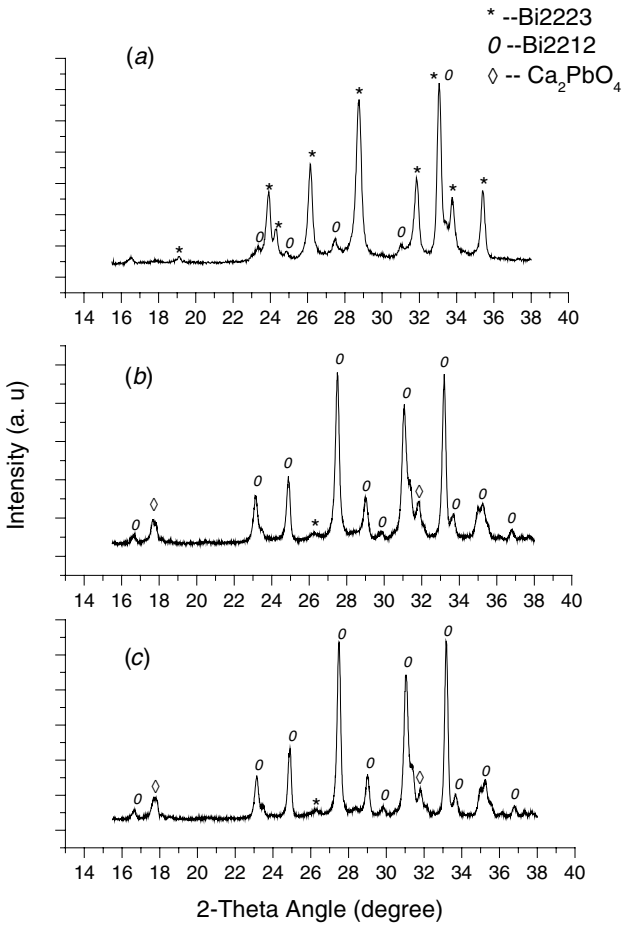

Figure 2. X-ray diffraction patterns of powders A (*a*), B (*b*) and C (*c*).

Process B. The raw powders were manually ground in an agate mortar and only calcined under air at 820 °C for 24 h.

Process C. The raw powders were mechanically mixed in air in an agate ball mill for 30 min and calcined under air at 820 °C for 24 h. The ball milling procedure is performed with the intention to avoid a significant presence of agglomerates, decrease the grain size and homogenize the powder. The particle size distribution of powders was analysed by a Mastersizer Malvern analyser for which, in order to disperse the agglomerates, the powders were subjected to an ultrasonic agitation in alcohol prior to their insertion in the sample cell. The particle size distributions of powders B and C before the calcination are presented in figure 1. The effect of ball milling on the grain size is clearly significant after 30 mn of treatment.

XRD patterns of the three powders are shown in figure 2. Powder A is characterized by a large amount of Bi2223, whereas powders B and C exhibit an assemblage composed mainly of Bi2212 and secondary phases such as Ca_2PbO_4, CuO, Ca_2CuO_4 or $Sr_{14}Cu_{24}O_{41}$. No significant difference exists between the XRD patterns of powders B and C, neither in phase content nor in peak broadening. This suggests that our ball-milling procedure did not significantly affect the kinetic formation of the different phases during the calcination, nor did it induce any particular crystallite size.

The well-established sinter-forging method was used to fabricate superconducting discs. The processed powders were cold-pressed into 2 mm thick and 25 mm diameter pellets, under an uniaxial pressure of 23 MPa which resulted in a green density of 60% of the theoretical value. The pellets were then placed into the furnace under air atmosphere [16] between two 0.125 mm thick silver sheets to avoid reaction with the alumina supports during heating. The pressure employed was fixed at 30 MPa, and the operating temperature ranged between 838 °C and 855 °C, using 20, 50 and 100 h plateaus. This sinter-forging temperature range corresponds partially to the Bi-2223 phase formation domain [17]. The furnace was turned off just after the pressure release to fix the equilibrium phases and to minimize any decomposition into secondary phases at low temperature. The approximate rate of quenching is 400 °C h^{-1}. The discs were cut into sticks and annealed under 7.5% O_2 at 820 °C for 100 h, cooled at 1 °C h^{-1} to 800 °C and then quenched to room temperature.

XRD measurements were performed on a 4-circle X'PERT Philips goniometer in the Bragg–Brentano geometry. The incident plane of the x-rays was positioned parallel to the cylinder axis of the samples. A first azimuthal scan (φ-scan) was operated on the (119) reflection in order to check for specific texture symmetries. As expected for uniaxially deformed materials without subsequent growth, a C_∞ axis of symmetry aligned with the cylinder axis was detected, as reported by other authors [18]. Then tilt scans (ψ-scans) were performed from $\psi = 0°$ to $\psi = 85°$ in steps

of 5°. However, in such materials the presence of several low crystal-symmetry phases makes the texture analysis a complex problem when working with a point detector. Strong peak overlaps occur, which makes it difficult to distinguish whether the observed signal is actually composed of one reflection or several, and from a single phase or not. This is particularly true at high ψ values for which high beam defocusing arises. One way to overcome this problem is to use a position sensitive detector (PSD) and treat the diagrams in order to deconvolute the different signals from the different phases [19]. In the absence of a PSD, θ–2θ scans were measured from 21.5° to 25.5° (width = 0.02°) in order to encompass the (008) and (00$\underline{10}$) reflections of Bi2212 and Bi2223, respectively. The two contributions were deconvoluted by fitting the x-ray profiles using a Pseudo-Voigt peak shape for each ψ position of the sample. A 0.5 mm × 0.5 mm collimated beam and a low vibration of the sample holder (1 mm) were used in order to ensure both that the beam remained focused on the sample in the analysed 2θ range (even at high sample tilts) and that the number of irradiated crystallites was statistically relevant (more than 30 000 grains were probed under these conditions). The integrated areas from these scans were used to reconstruct ψ-scans which represent the {00l} plane dispersions of the crystallites. These were then fitted as Gaussian orientation distributions and normalized into distribution densities by direct normalization procedure [20], and the full width at half maximum (FWHD) of the distribution densities was used as a quantitative appreciation of the crystallite dispersion.

The volume percentage of Bi2223 and Bi2212 phases were calculated on the basis of the corresponding {00$\underline{10}$} and {008} pole figures, obtained from the distribution density scans. Indeed, from only classical θ–2θ scans, one cannot accurately estimate the phase contents of textured materials, since diffracted intensities are affected by the texture itself, which is *a priori* unknown for all phases. Furthermore, the texture of the different phases may be different. Thus, the measured and normalized pole figures were integrated in order to sum the reflection contributions over the sample orientations. The volume percentage was then calculated from these integrated intensities and the structure factors of the corresponding lines.

Using this procedure, we were able to determine orientation volumic fractions of less than 1% with a resolution of approximately ±0.1%, on thin films of the YBCO compounds [21]. It is then assumed here that our resolution is of the same order for crystalline phases, since all the phase of concerns exhibit similar scattering power. Amorphous phases, which would be more difficult to detect by x-rays, are not expected at the used annealing temperature, and we did not see any background modulation that could be associated with it.

Transport critical current densities (J_c) of 10 × 2 × 0.2 mm^3 samples were characterized by the standard four-probe technique at 77 K without magnetic field and with an electric field criterion of 1 μV cm^{-1}. The magnetization was measured using a SQUID magnetometer. The dimensions of the samples were about 4 × 1.5 × 0.2 mm^3. Microstructures of the powder were analysed with a Philips XL 30 FEG scanning electron microscope (SEM).

3. Results and discussion

3.1. Influence of precursor powder

3.1.1. Sinter-forging and phase formation. XRD patterns of discs textured at 838, 845 and 850 °C for 20 h using powders A, B and C are presented in figure 3. By comparing the relative intensities of the (008)-2212 ($2\theta \approx 23.1°$) and the (00$\underline{10}$)-2223 ($2\theta \approx 23.9°$) peaks, it is clear that the three starting powders have different effects on the evolution of the Bi2223 phase content for each powder type.

Powder A. As observed in a previous work [3], the Bi2223 phase is present in a large quantity in all samples, which proves that the load applied during the sinter-forging technique does not destroy the Bi2223 phase initially stabilized during the sintering steps. It is interesting to note that the Bi2212 phase is present in the sample textured at 838 °C, although in a relatively small amount, whereas the samples textured at 845 °C and 850 °C exhibit only the Bi2223 phase peaks. The combination of appropriate sinter-forging temperature and pressure allows the nearly complete formation of the Bi2223 phase, even if some residual Bi2212 was present in the mixture before sintering (figure 2). The contact between grains of superconducting and secondary phases is considerably enhanced by grain sliding and stacking during sinter-forging, whereas a simple sintering step induces a retrograde densification [22] and limits the complete Bi2223 phase formation. The presence of the Bi2212 phase in the samples textured at 838 °C is also associated with the $(Pb,Bi)_3Sr_2Ca_2CuO_y$ (Bi3221) phase. Traces of Bi3221 have been reported in fully reacted Bi2223 compounds by several authors [23–25]. In this case, the Bi2223 phase has not been completely formed and secondary phases still coexist with the Bi2223 and Bi2212 phases at lower sintering temperatures. Otherwise, at temperatures higher than 850 °C, the Bi2223 phase begins to decompose into a liquid phase, leading to an inhomogeneous and decomposed sample, hardly separable from the silver sheets without breaking. The reaction between the silver sheets and the liquid phase hinders the alignment between the plate-like grains, and the resulting powder morphology displays large grain boundaries and poor grain connectivity. Thus it can be concluded that, using highly pure Bi2223 powder, the sinter-forging process is optimal in the temperature window of 845–850 °C, for which nearly pure Bi2223 is obtained. These conclusions are in agreement with results reported from another previous work in which the optimal processing in air occurred at 845–850 °C [26].

Powder B. After 20 h of heat treatment and pressing, the Bi2212 phase was partially converted into Bi2223 (figure 3). The relative intensities between the (008)-2212 and (00$\underline{10}$)-2223 peaks show that the Bi2223 phase content is weakly dependent on the sintering temperature. Furthermore, no significant difference exists in the XRD patterns in terms of superconducting and secondary phases. Tests at temperatures higher than 850 °C induce the formation of a large amount of liquid phase which reacts with the alumna support. The resulting discs are not exploitable due to contamination.

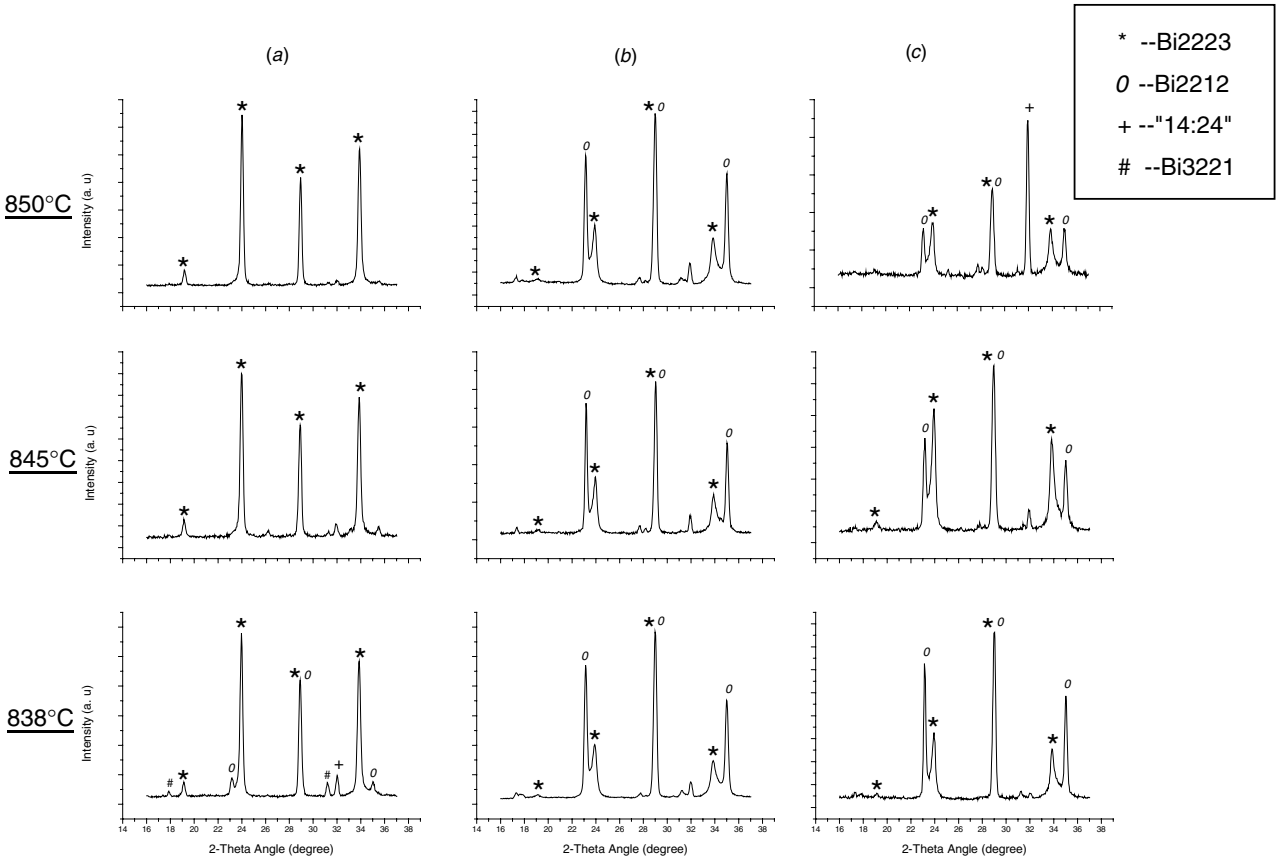

Figure 3. XRD patterns of discs textured at 838, 845 and 850 °C for 20 h using powders A (*a*), B (*b*) and C (*c*).

Powder C. Contrary to powder B, the XRD patterns of the discs textured at various temperatures using powder C as a starting precursor exhibit strong differences. The Bi2223 phase formation is highly sensitive to the temperature. A large increase of the Bi2223 phase content at temperatures higher than 838 °C is clearly observed, as the presence of a strong peak indexed in the $Sr_{14}Cu_{24}0_{41}$ structure ($2\theta \approx 32°$) in discs textured at 850 °C. Temperatures above 850 °C also induce degrading reactions.

Powders A, B and C were designed to explore the effect of calcination and intermediate grindings on the phase formation and final properties of textured discs. Powder A contains a large amount of Bi2223 phase, whereas powders B and C are composed principally of Bi2212 and present nearly the same XRD pattern. However, comparing the XRD intensities of discs textured at different temperatures (figures 3(*b*) and (*c*)), it is obvious that the conversion rates of the Bi2212 to Bi2223 are quite different in discs textured from powder B or C. This implies that the formation rate of the Bi2223 phase depends on the intermediate ball milling performed before the calcination, which affects the reactivity, homogeneity, assemblage or some other factor that influences the kinetic phase formation during the texturation step.

The first possible cause is the influence of the grain size of the calcined powders. However, each powder has been ground manually after the calcination and sieved at 63 μm. In figures 4(*a*) and (*b*), the particle size distributions of powders B and C after calcination are shown. They exhibit no significant difference, except that powder C shows a larger amount of particles in the range 10–60 μm and under 1 μm. This difference is probably due to ball milling applied before the calcination step, which creates a finer powder with a higher reactivity and leads to the production of liquid phase during the calcination. The powder at the bottom of the crucible forms a 'cake' with a strong cohesion of Bi2212 platelets due to the solidification of the liquid phase, whereas, at the surface, the powder is composed typically of Bi2212 platelets and secondary phases. Figure 5 shows the SEM images of the Bi2212 platelet grains of powder B or C (figure 5(*a*)), and of the solidified liquid phase present only in powder C (figure 5(*b*)). The subsequent manual grinding carried out between the calcination and the texturation steps broke up the 'powder cake' composed of Bi2212 and the solidified liquid phase, leading to the formation of dense agglomerates with greater hardness.

Consequently, the increased amount of Bi2223 obtained from the samples textured using powder C is not due to smaller grains but due to the presence of a large amount of liquid phase produced during calcination. During the texturation step, the solidified liquid melts again, which promotes elemental diffusion and improves the Bi2223 phase formation. Formation kinetics are highly sensitive to temperature, resulting in significantly different Bi2223 phase content in samples textured at slightly different temperatures (figure 3(*c*)). In conclusion, ball milling before the calcination seems necessary to homogenize the powder, increase its

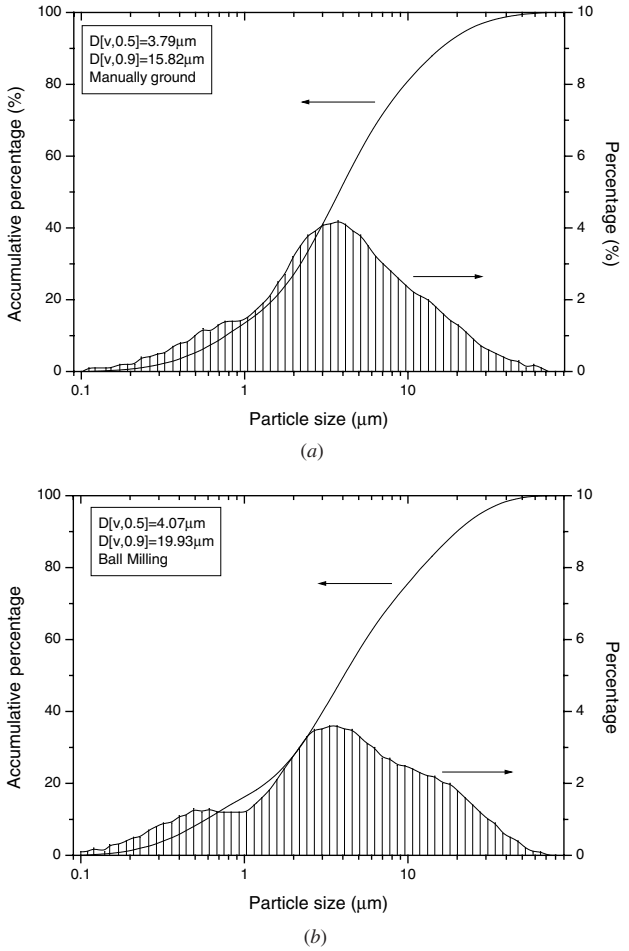

Figure 4. Particle size distributions of powders B (*a*) and C (*b*) after calcination.

reactivity and produce a large amount of liquid phase which promotes the Bi2223 phase formation during the texturation step.

3.1.2. Critical current densities

(a) Evolution of J_c for each process. The J_c values of discs made from the three powders at different sinter-forging temperatures are given in table 1. The sinter-forging time was fixed at 20 h. Higher J_c values are achieved for powder C at sinter-forging temperatures of 838 °C and 845 °C. At temperatures higher than 845 °C, the critical current density decreases drastically, probably due to the presence of $Sr_{14}Cu_{24}O_{41}$ (figure 3(*c*)). The latter phase could also explain the low J_c value of powder C processed at 850 °C. For the discs made from powder B, the J_c values are lower than those obtained with powder C and are insensitive to the processing temperature. This behaviour is in agreement with XRD patterns of discs textured at 838, 845 and 850 °C (figure 3(*b*)) which exhibit no significant differences. The samples prepared from powder A show an increase of J_c when the processing temperature increases. Such evolution has been proved to be correlated to the presence of Bi2212 and Bi3221 phases [3]. Heat treatment conditions were optimized around 845–850 °C for which pure and highly oriented Bi2223 discs are obtained.

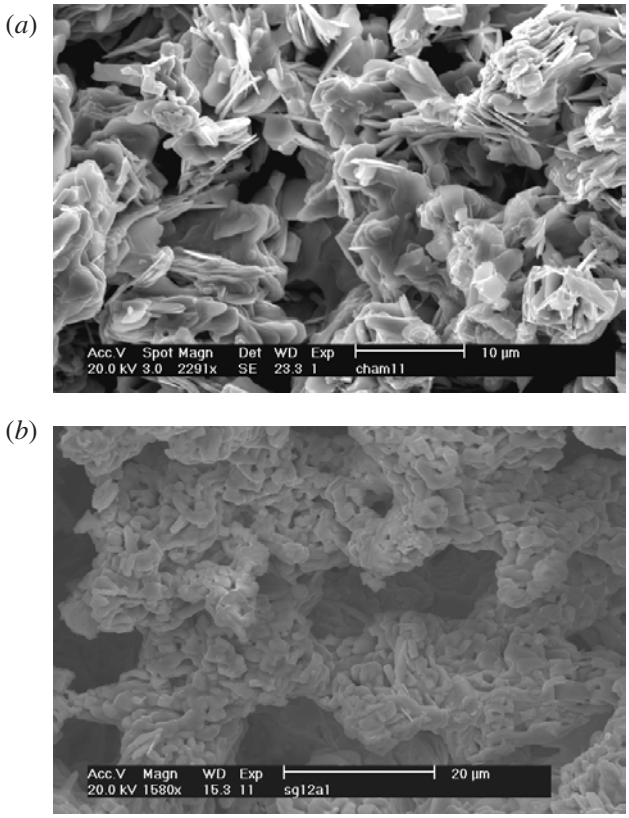

Figure 5. SEM images of Bi2212 platelet grains present in both powders B and C (*a*), and solidified liquid phase present only in powder C (*b*).

Table 1. J_c values of discs made from the three powders with different sinter-forging temperatures.

		838 °C	845 °C	850 °C
J_c (A cm^{-2})	Powder A	6 822	9 913	10 600
	Powder B	7 024	7 112	6 320
	Powder C	13 472	14 225	8 706

Table 2. Comparison of the critical current densities and Bi2223 phase content with the FWHD values for samples textured at 845 °C for 20 h.

	J_{cT} (A cm^{-2})	FWHD (°)	% Bi2223
Powder A	9 913	25.96	70
Powder B	7 112	18.6	17.67
Powder C	14 225	19.17	32.08

(b) Comparison of J_c values. Comparison between samples A and B (or C). Comparison of the XRD analysis in figure 3 and the final critical current densities shows that powder C exhibits the highest critical current densities, although its Bi2223 phase content is lower than in samples textured using powder A. This is in agreement with sharper orientation distributions obtained in sample C. Table 2 shows the comparison of the critical current densities and Bi2223 phase content with the FWHD values for samples textured at 845 °C for 20 h. It is clear that powders B and C lead to smaller FWHD values than powder A. This result is due to the precursor phase assemblage. Instead of starting with a highly pure Bi2223 powder (powder A), the solution to form Bi2223 discs with the highest orientation

(*a*)

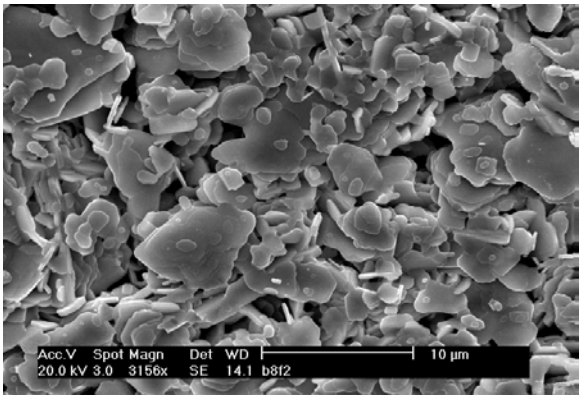

(*b*)

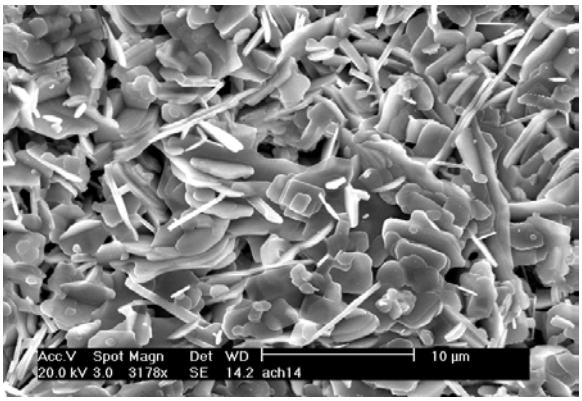

Figure 6. Microstructure of pellets sintered in the range 840–845 °C for 20 h and composed of powders A (*a*) and B (*b*).

degree is to start with calcined powders (powders B and C). At a high temperature, the secondary phases melt and, consequently, the plate-like grains grow and reorient easily because of the large amount of liquid phase. In this case, the absence of secondary phases in powder A is a limiting factor for the improvement of the alignment of platelet grains and leads to high FWHD values. It can be concluded that the major factors in achieving strong critical current densities are not only the Bi2223 phase content but also the grain alignment. Comparing results of samples A and C, it is obvious that the decrease of Bi2223 content has less influence than the decrease of FWHD on the final J_c values in this content range.

The microstructure of pellets sintered in the range 840–845 °C for 20 h and composed of powders A and B (or C) are presented in figures 6(*a*) and (*b*), respectively. This heat treatment, comparable to a sinter-forging cycle without uniaxial pressure, was performed in order to observe the grain growth of each powder. The platelet grains in figure 6(*a*) are larger than in figure 6(*b*) and are also more oriented with respect to plane surface of the pellet. This implies that the sintering treatments used to synthesize the Bi2223 powder (i.e. powder A) lead to the formation of large grains ($\phi > 10$ μm). These grains are difficult to orient during the texturation step, and especially, in the absence of secondary phases, which results in texture characterized by lower distribution densities, i.e. higher FWHD values.

Comparison between samples B and C. Powder B exhibits a lower Bi2223 content and a FHWD value close to that of powder C. SEM observations (figure 5(*b*)) show the presence of a large amount of liquid phase in powder C which, as previously described, results in faster Bi2223 phase formation for similar starting grain sizes (figures 4(*a*) and (*b*)). Thus, it can be supposed that the high critical current densities of discs textured using powder C are due to a higher Bi2223 content as well as a strong grain connectivity and orientation related to the presence of a large liquid phase content.

3.2. Study of discs textured via process C

Figure 7 shows the XRD patterns of discs textured at 838, 845 and 850 °C for various durations. For each temperature, the Bi2223 phase content increases as the sintering time increases. In the case of discs textured at 845 °C, the volume percentages of Bi2223 and Bi2212 phases calculated on the basis of the corresponding {00$\underline{10}$} and {008} pole figures are equal to 32 and 68%, respectively, for 20 h and approach 59% and 41% for 100 h. Another interesting observation is the evolution of the Bi2223 phase content in the case of discs textured at 838 °C. Although the percentage of Bi2223 is relatively low for a 20 h texturation cycle, it increases rapidly after 50 h of texturation and reaches 60% after 100 h. A hypothesis to explain such a behaviour is based on the elemental diffusion. In the first hours of texturation, at a reaction temperature as low as 838 °C, the diffusion is not yet completely achieved due to a high liquid viscosity and a low connectivity between grains. After 50 h of texturation, the platelet grains are stacked and the density approaches the theoretical value, the elemental diffusion becomes easier, and the Bi2223 phase formation is activated. Discs textured at 838 °C, 845 °C or 850 °C reach approximately the same Bi2223 phase content after 100 h of heat treatment. But for only 20 h of reaction at 850 °C, the main peaks from the $Sr_{14}Cu_{24}O_{41}$ (or 14, 24) phase are strong. This result confirms conclusions of the paper by Giannini *et al* [27] in which it is shown that the formation of (14, 24) is fast at a high temperature. During the heating step, the (14, 24) phase content increases and saturates when the dwell temperature is attained. Maintaining the temperature constant then induces a decrease in (14, 24) phase. In our case, the decrease of the (14, 24) peak intensity with increasing sinter-forging times is also observed and proves that the formation of Bi2223 is correlated to the consumption of the (14, 24) phase.

Figure 8 shows the evolution of J_c of the discs textured at 838 °C, 845 °C and 850 °C during 20, 50 and 100 h. It is clear that, at all temperatures, the J_c value increases with sinter-forging time. The critical current densities obtained around 19 000–20 000 A cm^{-2} represent a real improvement in the optimization of transport properties in the case of bulk Bi2223 textured using the sinter-forging process. To our knowledge, the largest J_c value obtained before now saturated around 10 000–12 000 A cm^{-2} [1–3, 5] and required a long sintering step to form the Bi2223 phase. With the calcination–sinter-forging (CSF) cycle, values larger than 13 000 A cm^{-2} can be reached after only 40 h. This result is mainly due to the improvement of the texture quality, i.e. low FWHD values, caused by the modification of the starting precursor and to a larger extent due to the presence of a large amount of liquid phase during the texturation. Furthermore, the temperature window used to attain these high critical current density values is between 838 and 850 °C, which is sufficiently

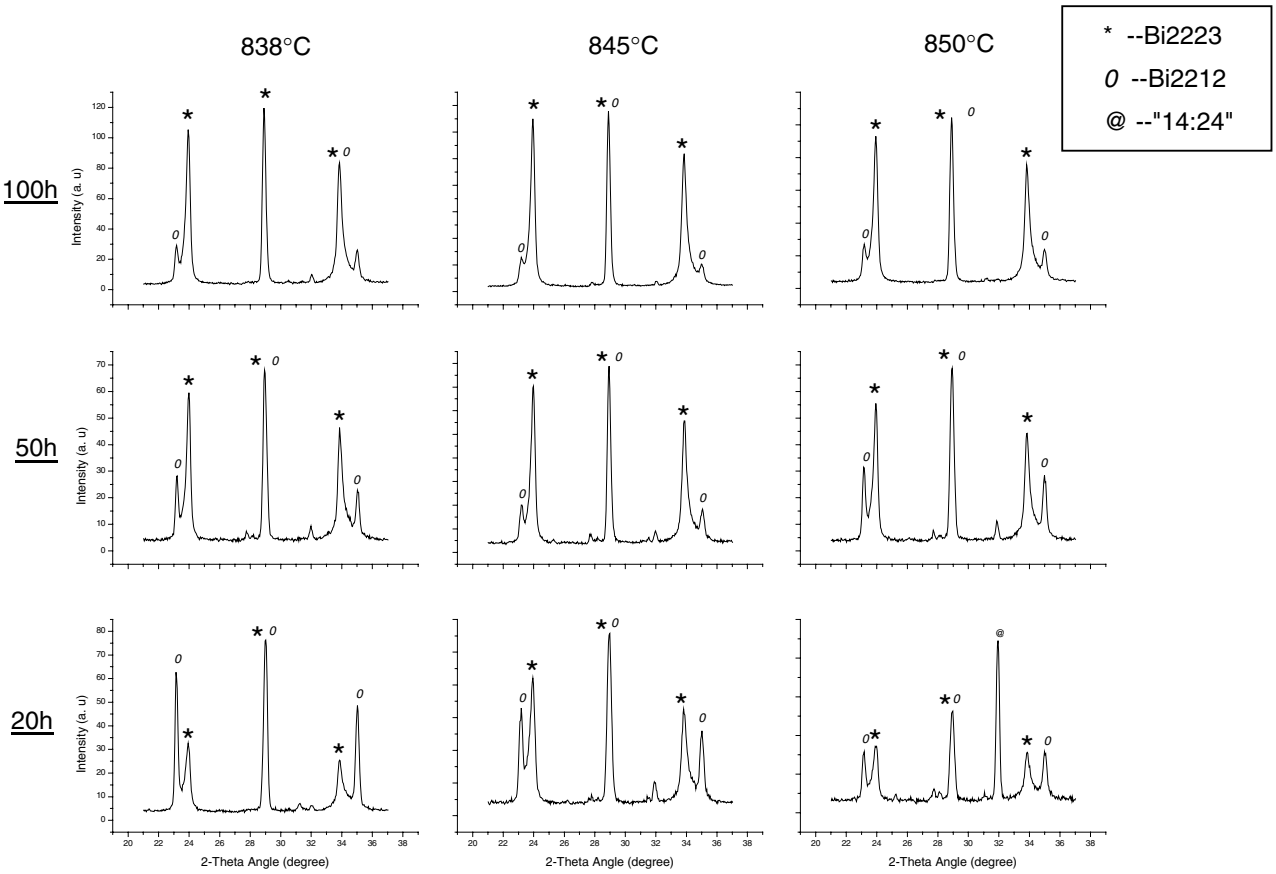

Figure 7. XRD patterns of discs textured from precursor powder C at 838, 845 and 850 °C for 20, 50 and 100 h.

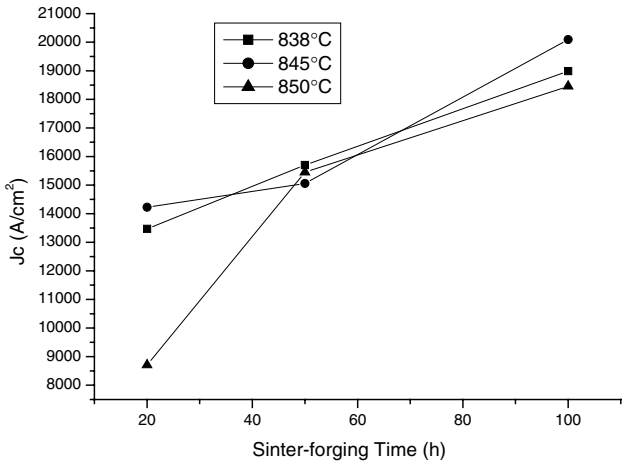

Figure 8. Evolution of J_c of the discs textured from precursor powder C at 838, 845 and 850 °C for 20, 50 and 100 h.

large to fabricate bulk samples with reproducible properties. Nevertheless, the formation of the Bi2223 phase is still rather slow and other studies are necessary to promote its growth. The modification of the precursor powder could be a possible way. For instance, Dorris *et al* [28, 29] showed that starting with Pb-doped Bi2212 is favourable to obtain a highly pure Bi2223 powder in short times.

Figure 9 presents the crystallite distributions of the Bi2212 and Bi2223 phases and the Bi2223 content of the discs textured at 845 °C for 20, 50 and 100 h using powders B and C. Two different trends can be observed. In figure 9(*a*), the FWHD of the Bi2212 phase increases with the increasing sinter-forging time, while the FWHD of the Bi2223 phase decreases. Similarly, the Bi2223 phase content increases with increasing sinter-forging time. A strong reverse correlation between the decrease of FWHD of Bi2223 and the formation of this phase is observed, which is synonymous of its strong growth anisotropy leading to a favourable orientation of crystallites. After nucleation, the growth stage of Bi2223 is responsible for the texture stabilization. Simultaneously, we note a small FWHD increase of the Bi2212 phase. This seems to indicate that the Bi2223 formation and growth is associated with a weak perturbation in the orientation of Bi2212. Such observations have led, in a previous work, to the conclusion that the transformation mechanism is probably a nucleation-growth model with the decomposition of the Bi2212 and the growth of the Bi2223 phase.

In figure 9(*b*), the FWHD values of the Bi2212 and the Bi2223 phases decrease jointly while the Bi2223 phase content increases with increasing sinter-forging times. Two points must be clarified. Firstly, after a 20 h sinter-forging cycle, the FWHDs of the two phases are nearly equal to their counterparts in figure 9(*a*). This means that, in the first 20 h, samples B and C are not significantly different in terms of crystallite orientations. Secondly, the inverse evolution of the FWHD values of Bi2223 and Bi2212 (figure 9(*a*)) is no longer observed in figure 9(*b*), but the two FWHDs evolve

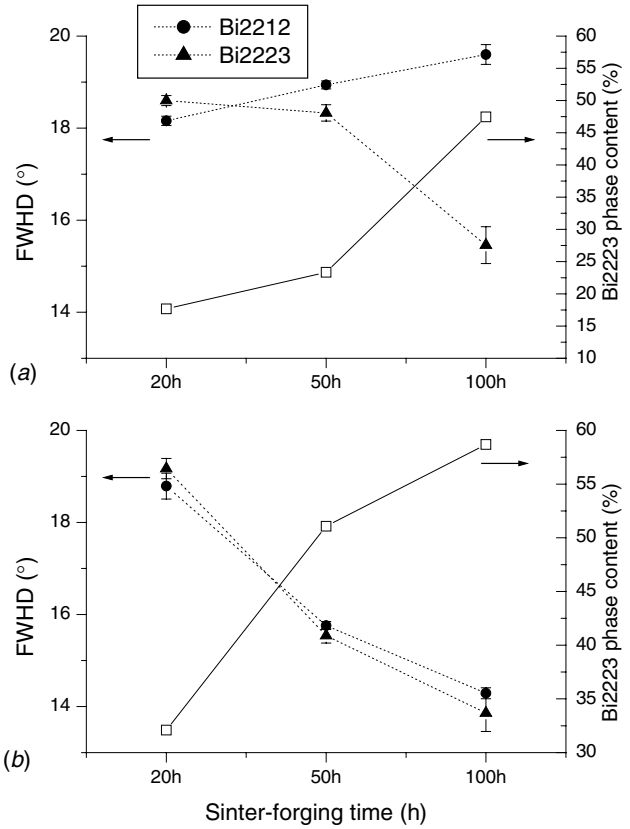

Figure 9. Crystallite distributions of the Bi2212 and Bi2223 phases, and Bi2223 phase content of discs textured at 845 °C during 20, 50 and 100 h using powders B (*a*) and C (*b*).

contiguously whatever the sinter-forging time is. Furthermore, after 50 h, the texture strengths of both phases are larger than in sample B with FWHD values as low as 14°. It is suspected that the phase assemblage of the precursor powders is the cause of this effect. The large content of solidified liquid phase probably eases sliding and stacking of grains which improved intergrain connections, a high texture degree and, consequently, high critical current densities.

4. Conclusion

The influence of starting precursor powders on the transport properties and texture quality of samples prepared by the sinter-forging method has been studied. Maximum J_c was attained from a precursor powder that consisted of Bi2212 plus non-superconducting phases with an intermediate ball milling before the calcination. The resulting critical current densities of 19 000–20 000 A cm^{-2} represent a great improvement in the optimization of transport properties in the case of bulk Bi2223 textured using the sinter-forging process. This result is mainly due to the improvement of the texture strength, i.e. low FWHD values, caused by the modification of the starting precursor and also due to the presence of a significant concentration of liquid phase during the texturation.

Acknowledgment

E Guilmeau is grateful to le Ministère de la Recherche et de la Technologie for his PhD fellowship.

References

[1] Rouessac V, Poullain G, Provost J, Gomina M and Desgardin G 1998 *Eur. Phys. J.* **AP 2** 145
[2] Tampieri A, Celotti G, Calestani G and Lesca S 1997 *Key Eng. Mater. Euro Ceramics V* **132** 1247
[3] Guilmeau E and Noudem J G 2002 *Supercond. Sci. Technol.* **15** 1566
[4] Murayama N and Vander Sande J B 1995 *Physica* C **241** 235
[5] Guilmeau E, Chateigner D and Noudem J G 2002 *Supercond. Sci. Technol.* **15** 1436
[6] Wang M, Xiong G, Tang X and Hong Z 1993 *Physica* C **210** 413
[7] Murashov V A, Ionescu M, Murashova G E, Dou S X, Liu H K and Apperley M 1997 *Inst. Phys. Conf. Ser.* **158** 937
[8] Chen F H, Koo H S and Tseng T Y 1991 *Appl. Phys. Lett.* **58** 637
[9] Shi D, Boley M S, Chen J G, Xu M, Vandervoort K, Liao Y X and Zangvil A 1989 *Appl. Phys. Lett.* **55** 699
[10] Uzumaki T, Yamanaka K, Kamehara N and Niwa K 1989 *Japan. J. Appl. Phys.* **1** 75
[11] Morgan P E D, Piche J D and Housley R M 1992 *Physica* C **191** 179
[12] Murayama N and Vander Sande J B 1996 *Physica* C **256** 156
[13] Rouessac V, Wang J, Provost J and Desgardin G 1996 *J. Mater. Sci.* **31** 3387
[14] Garnier V, Monot I and Desgardin G 2000 *Supercond. Sci. Technol.* **13** 602
[15] Guilmeau E, Andrzejewski B and Desgardin G 2002 *Physica* C **377** 304
[16] Rouessac V, Wang J, Provost J and Desgardin G 1996 *Physica* C **268** 225
[17] Strobel P and Fournier T 1990 *J. Less-Common Met.* **164** 519
[18] Wenk H-R, Chateigner D, Pernet M, Bingert J, Hellstrom E and Ouladdiaf B 1996 *Physica* C **272** 1
[19] Ricote J and Chateigner D 1999 *Boletín de la Sociedad Española de Cerámica y Vidrio* **38** 587
[20] Manceau A, Lanson B, Chateigner D, Wu J, Huo D F, Gates W P and Stucki J W 2000 *Am. Mineral.* **85** 153
[21] Pernet M, Chateigner D, Germi P, Dubourdieu C, Thomas O, Sénateur J P, Chambonnet D and Belouet C 1994 *Physica* C **235–240** 627
[22] Thayer R L, Scmidt S R, Dorris S E, Bullard J W and Lanagan M T 2000 *J. Am. Ceram. Soc.* **83** 2365
[23] Wang W G, Horvat J, Li J N, Liu H K and Dou S X 1998 *Physica* C **297** 1
[24] Liu H K, Horvat J, Bhasale R, Wang W G, Zeimetz B, Dou S X, Kusevic I and Babic E 1998 *Supercond. Sci. Technol.* **11** 1057
[25] Lehndorff B, Hardenbicker P, Hortig M and Piel H 1999 *Physica* C **312** 105
[26] Chen N, Biondo A C, Dorris S E, Goretta K C, Lanagan M T, Youngdahl C A and Poeppel R B 1993 *Supercond. Sci. Technol.* **6** 674
[27] Giannini E, Bellingeri E, Passerini R and Flükiger R 1999 *Int. J. Mod. Phys.* B **13** 1067
[28] Dorris S E, Prorok B C, Lanagan M T, Sinha S and Poeppel R B 1993 *Physica* C **212** 66
[29] Dorris S E, Prorok B C, Lanagan M T, Browning N B, Hagen R, Parrell J A, Feng Y, Umezawa A and Larbalestier D C 1994 *Physica* C **223** 163